Zr and Hf microalloying in an Al-Y-Fe amorphous alloy. Relation between local structure and glass-forming ability

Anne Sadoc, Maher Sabra, Olivier Proux, Jean-Louis Hazemann, Karyn Spence, Kenneth Franklin Kelton

Zr and Hf microalloying in an Al-Y-Fe amorphous alloy. Relation between local structure and glass-forming ability

Journal:	*Philosophical Magazine & Philosophical Magazine Letters*
Manuscript ID:	TPHM-08-Feb-0036.R2
Journal Selection:	Philosophical Magazine
Date Submitted by the Author:	02-Aug-2008
Complete List of Authors:	Sadoc, Anne; Université de Cergy-Pontoise, Physique/LPMS Sabra, Maher; Université de Cergy-Pontoise, Physique/LPMS Proux, Olivier; ESRF Hazemann, Jean-Louis; ESRF Spence-Bondi, Karyn; Washington University, Department of Physics Kelton, Kenneth; Washington University, Physics
Keywords:	amorphous alloys, EXAFS, nanostructures
Keywords (user supplied):	microalloying, Al-Y-Fe

Philosophical Magazine
Vol. X, No. X, Month 200X, 000–000

ARTICLE

Zr and Hf microalloying in an Al-Y-Fe amorphous alloy. Relation between local structure and glass-forming ability

A. SADOC*,[1], M. SABRA[1], O. PROUX[2,3], J.-L. HAZEMANN [2,4], K. S. BONDI [5] and K. F. KELTON [5]

[1] LPMS, Université de Cergy-Pontoise, Neuville sur Oise, 95031 Cergy-Pontoise Cedex, France.

[2] CRG-FAME beamline, ESRF, BP 220, 38043 Grenoble Cedex

[3] Laboratoire de Géophysique Interne et Tectonophysique, 1381, rue de la Piscine, 38400 Saint-Martin-D'Hères

[4] Institut Néél, 24 avenue des Martyrs BP 166, 38042 Grenoble Cedex 09

[5] Department of Physics, Washington University, St. Louis, MO 63130, USA.

* Corresponding author. E-mail: Anne.Sadoc@u-cergy.fr

Philosophical Magazine
Vol. X, No. X, Month 200X, 000–000

ARTICLE

Zr and Hf microalloying in an Al-Y-Fe amorphous alloy. Relation between local structure and glass-forming ability

Abstract

The effects of the addition of small amounts of Zr and Hf (0.5 - 3 %) on the atomic structure of $Al_{88}Y_7Fe_5$ metallic glass were examined from extended x-ray absorption fine structure (EXAFS) experiments to better understand the influence of these microadditions on the glass forming ability of this alloy. Measurements at the Zr K and Hf LIII absorption edges have allowed the local structures around Zr and Hf atoms to be determined. The same Al environment was found for the different concentrations, consisting of a small cluster extending up to 4.5 Å around the Zr atoms and up to 6 Å around the Hf ones. Although the clustering effect is smaller in the Zr neighbourhood, a drastic shortening of the nearest Zr-Al distance is shown, providing evidence for some covalent character to the bonding, in line with the increased glass-forming ability found in the alloys made with the Zr microaddition.

Keywords: nanostructure, microalloying, Al-Y-Fe, EXAFS.

PACS numbers: 61.43.Dq, 61.46.-w, 61.10.Ht.

1. Introduction

Due to the considerable scientific and technological importance of bulk metallic glasses, a significant effort has been devoted to the investigation of the unusual glass-forming ability found in some metallic alloys with microalloying [1-6]. This cannot be explained well by often-cited theories and empirical rules for metallic glass formation, but can be attributed to an increase of the short-range ordering in the alloys.

The Al-Rare Earth-Transition Metal (Al-RE-TM) glasses with a high Al content, discovered by He et al. [7] and Tsai et al. [8], are particularly intriguing. Their significant improvement in strength over conventional Al-based crystal alloys and their high ductility suggest potential aerospace and other applications [9]. The reasons for glass formation in these alloys are unclear. They differ from traditional metallic glasses and from most of the recently discovered bulk metallic glasses, not forming near deep eutectics in the phase diagram for example. It is, therefore, of both fundamental and practical interest to understand the formation and mechanism of microalloying in these glasses.

Recently, it was reported that the addition of as little as 0.5 at.% of Ti or V dramatically improves glass formation in $Al_{88}Y_7Fe_5$ alloys and changes the subsequent crystallization processes [10,11]. Based on EXAFS measurements, we have studied the short-range order in these alloys [12]. These measurements have demonstrated for the first time, to our knowledge, that a well-defined Al nanostructure exists around the V and Ti atoms, the alloying elements, which is different from that around the Al, Y and Fe atoms, the major alloy constituents, even at the lowest concentrations. The local structure around the microadditions is also different from that of the primary crystallizing phase, α-Al, demonstrating a structural basis for the improved glass formation with microalloying in the Al-Y-Fe alloys. Moreover, the measurements showed that Ti and V form strong interactions with Al, with a significant

shortening of the bond length. This could raise the barrier for nucleation of α-Al and decrease the atomic mobility of Al, explaining the greater stability of the glasses containing Ti or V.

Here we continue the exploration of the structural role of microadditions on glass formation in Al-Y-Fe alloys. Using EXAFS measurements at the Zr K and Hf LIII absorption edges, we have investigated the local atomic structures in alloys prepared with small additions of Zr (0.5, 1 and 2 %) or Hf (1, 2 and 3 %). The results are compared to previous ones obtained in $Al_{88}Y_7Fe_5$ with and without Ti or V.

The paper is organised as follows. The sample preparation and the EXAFS experiments are described in section 2. The EXAFS analysis is presented in section 3. The local structure around the Zr and Hf atoms is discussed in section 4 for the different samples. A general discussion of the results appears in section 5 and a summary and conclusion are presented in section 6.

2. Experimental methods

Samples of $Al_{88-x}Y_7Fe_5Zr_x$ (with x = 0.5, 1 and 2) and $Al_{88-x}Y_7Fe_5Hf_x$ (with x = 1, 2 and 3) were prepared and characterised at Washington University [10]. Alloy ingots of the desired composition were first produced by arc-melting mixtures of the pure elements on a water-cooled copper hearth in a high purity argon atmosphere. A Ti-getter located close to the samples was melted prior to arc melting to further remove oxygen from the chamber. To ensure a homogeneous composition, samples were arc melted three times. Amorphous ribbons were prepared by melting the ingots using rf-induction heating to 1100-1150 °C (well above the liquidus temperature) in a graphite crucible under an Ar atmosphere, and the liquid was rapidly quenched onto a rotating copper wheel. The quenched ribbons were 1-2 mm wide and 20-30 μm thick. Samples were characterized by X-ray diffraction and differential

scanning calorimetry (DSC).

The EXAFS experiments were performed on the ribbons, which were impossible to crush or grind due to their amorphous structures. The studies were carried out at the European Synchrotron Radiation Facility (ESRF, Grenoble). The Zr K absorption edge (17997 eV) and the Hf LIII absorption edge (9561 eV) were probed on the CRG-FAME (BM30B) beam line [13]. The spectra were collected in the fluorescence mode with a Si (220) double-crystal monochromator at room temperature. The intensity of the fluorescence beam (I_f) was measured with a 30-element energy-resolved fluorescence detector. For reference, pure metallic zirconium and hafnium foils were studied in transmission mode at room temperature. The intensity of the beam before (I_O) and after (I) the sample was measured with Si diode detectors collecting part of the transmitted beams scattered by air.

3. Results

3.1 *Differential Scanning Calorimetry*

X-ray diffraction data for all of the rapidly-quenched alloys showed the broad diffraction patterns characteristic of an amorphous phase. The DSC nonisothermal data for the alloys are shown in figure 1. Except for the alloys containing 2 at.% and 3 at.% Hf, a feature typically taken to be the glass transition is observed (figure 1.b), which is absent in the rapidly quenched $Al_{88}Y_7Fe_5$ alloy made without microadditions. Finally, instead of the peak expected for glass devitrification, isothermal DSC measurements of the $Al_{88}Y_7Fe_5$ alloy made without microadditions show a monotonically decreasing signal with time, possibly indicating the coarsening of a nanocrystal/amorphous composite [10]. In contrast, all alloys prepared with Zr or Hf microadditions show the expected nucleation and growth crystallization peak (figure

2). Collectively these x-ray diffraction and calorimetric results demonstrate that the rapidly-quenched alloys are amorphous. The absence of a glass transition in the alloys containing 2 at.% and 3 at.% Hf is unclear. To determine changes in the primary crystallization pathway with microalloying, x-ray diffraction studies were made on as-quenched samples that had been annealed partially through the crystallization peak in the DSC. The $Al_{88}Y_7Fe_5$ alloys made with no microadditions crystallize to α-Al. In contrast, the alloys made with Zr and Hf concurrently form α-Al and varying combinations of two metastable phases that were observed in recent devitrification studies of alloys made with 3d transition metal microadditions[14].

3.2 *EXAFS Results*

Standard procedures of normalization and background removal were followed to determine the EXAFS oscillations, χ, versus the energy, E, of the photoelectron from the absorption coefficient, $ln\ I_O/I$, in transmission mode or I_f/I_O in fluorescence mode using a software package [15]. The data were then converted to momentum space (k-space) using $\hbar^2k^2/2m=E-E_O$, where E_O is the threshold energy origin and k is the photoelectron wave vector. The normalized EXAFS signals, $k\chi(k)$, are compared in figure 3 for the Zr edge of the zirconium foil and $Al_{88-x}Y_7Fe_5Zr_x$ samples (x = 0.5, 1 and 2 %) and in figure 4 for the Hf edge of the hafnium foil and $Al_{88-x}Y_7Fe_5Hf_x$ (x = 1, 2 and 3 %) samples.

The EXAFS of the zirconium and hafnium foils show structured oscillations characteristic of a crystallised material, while the amplitudes of the signals for the glassy alloys decrease monotonically with increasing k, in the form of a damped sinusoid. The spectra for the Zr and Hf edges are similar in alloys containing different concentrations of these elements, but they are less structured than for the edges of the Ti and V additions

studied previously [12]. The intensities of the Zr and Hf spectra are also smaller by a factor of two than for Ti and V.

The Fourier transforms (FTs) of the normalized EXAFS signals, $k\chi(k)$, were computed using a Kaiser window (τ=3). The same k window, roughly from 2.8 to 12 Å^{-1}, was used for the Zr and Hf edges. The moduli of the FTs are compared in figure 5 for the Zr edge and in figure 6 for the Hf edge. Several remarks can be made. First, the FT also are very similar for the different concentrations. Secondly, the first neighbour peak clearly appears at shorter distances in the alloys than in the pure metals, indicating that the first interatomic distance is shorter in the alloys. Peaks of next nearest neighbours appear for the alloys, but they are smaller than in the case of Ti and V additions for which the FTs show second and higher order neighbour peaks, up to about 7 Å (uncorrected for phase shifts), even at small concentrations. The intensities of these higher order peaks are about 10% of the main peak intensities in the Zr and Hf containing ribbons, while they were more than 30% for the Ti and V additions. However, the peaks of even higher order neighbours are also much smaller for the zirconium and hafnium containing foils than for the titanium and vanadium ones.

The modulus of the Fourier transform (FT) is qualitatively similar to the radial distributions of the atoms neighbouring the absorbing atom (Zr or Hf). However, the peaks are shifted to lower R-distances, because of the phase shifts experienced by the photoelectron while scattering from the potentials of the absorbing atom and nearest neighbours. Due to these phase shifts, the shape of the modulus of the FT does not provide a simple explanation of the environments of the atoms or an interpretation of the evolutions of these environments. To obtain this information, simulations must be done.

4. Local structure around zirconium and hafnium atoms

The spectra were reconstructed using the following formula [16], which describes the EXAFS oscillations for a Gaussian distribution of neighbours around a central atom:

$$\chi(k)=S_0^2\sum_j \frac{N_j}{kR_j^2}F_j(k)\exp(-\frac{2R_j}{\lambda(k)})\exp(-2\sigma_j^2k^2)\sin(2kR_j+\varphi_j(k)). \quad (1)$$

The sum is taken over the *j* multiple scattering paths. R_j is the half path length, central atom-neighbour distance for single scattering. N_j is the scattering path degeneracy, number of equivalent neighbours for single scattering. $\lambda(k)$ is the electron mean free path. The Debye-Waller factor $exp(-2\sigma_j^2k^2)$ is a measure of both static and dynamic disorder of path *j*. S_0^2 accounts for the central atom inelastic losses. $F_j(k)$ is the backscattering amplitude experienced by the photoelectron while scattering from the neighbours, $\varphi_j(k)$ is the total phase shift due to the contributions from both the absorbing atom and the scattering atoms. The amplitudes and phase shifts were calculated using the FEFF code [17], and the fitting was done with the programs RoundMidnight [15].

Calculations for the zirconium and hafnium foils were made using multiple scattering contributions. The sum in equation (1) is taken over the different paths, taking into account their degeneracy. The structure of crystalline Zr (Hf) is hexagonal close packed, hcp, with 6 first neighbours at 3.23115 Å in the hexagonal plane and 6 at 3.17875 Å, out of the plane (Hf: 3.1967 and 3.1307 Å) [18]. The *R*-range that was fit in the FT was about 2 to 5.5 Å. All possible scattering paths in this distance range were considered. The fits, shown in figures 3 to 6, were done with 11 paths for the Zr foil and with 9 paths for the Hf one.

4.1 *Al-Y-Fe alloys*

Before presenting the results for the Al-Y-Fe alloys doped with Zr or Hf, the EXAFS results obtained previously for the pure $Al_{88}Y_7Fe_5$ alloy [12] are briefly sketched here. The first

neighbour environment of the Al and Fe atoms consists of one shell of Al atoms, respectively 12 Al at a distance of 2.77 Å and 9 Al at 2.46 Å. The Y first-neighbourhood is composed of 16 Al atoms in two shells, with 14.6 Al atoms at 3.11 Å and 1.4 Al atoms at 3.65 Å. These results are in good agreement with those obtained previously around the Y and Fe atoms by Saksl et al. [19]. Comparing the bond lengths to the sum of the atomic radii (R_{Al}= 1.43 Å, R_Y= 1.80 Å, R_{Fe}= 1.26 Å), the Al-Al, Y-Al and Fe-Al first distances are noticeably shorter than the sums of the atomic radii, respectively 2.86 Å, 3.23 Å, and 2.69 Å. The relative shortening is only 3% for Al and 3.7% for Y, but is as great as 8.5% for Fe. Using the model of Miracle et al. [20], the maximum geometrically allowed coordination, N_T, is about 13 around Al, 17 around Y and 11 around Fe for respectively atomic radius ratios r_i/r_{Al} about 1, 1.26 and 0.88. The experimental coordination numbers are slightly below the maximum coordination number except for the Fe atoms for which it is clearly smaller. Since the Al-Al bond length was determined, an effective atom radius can be obtained for Al and consequently for Y and Fe using the first Y-Al and Fe-Al distances (r_{eff} is 1.385 Å for Al, 1.725 Å for Y and 1.075 Å for Fe). Using these values, the effective radius ratios are 1.245 for Y and 0.78 for Fe; with this the maximum coordination number is unchanged for Y but decreases to 9.5 around Fe, in accordance to the experimental coordination. Therefore, the Al atoms appear efficiently packed around Al, Y and Fe in the Al-Y-Fe alloys.

4.2 *Al-Y-Fe alloys with addition of Zr or Hf*

The large number of free parameters involved in the fitting procedure often makes the EXAFS analysis for ternary or quaternary alloys difficult [21]. To reduce the number of parameters, additional constraints can be applied based on a pre-knowledge of the investigated structure. The constraints in the following analysis use previously obtained

information from studies of the Ti and V microadditions [12]. In these two cases, the EXAFS spectra could be simulated assuming only Al neighbours around the Ti and V; the addition of Y and Fe atoms did not improve the fit. Based on this, only Al neighbours were assumed in the following analysis. For the samples with Zr or Hf additions, the main peak in the FTs can be reconstructed with Al neighbours, one shell of neighbours around the Hf atoms (Al at 2.78-2.80 Å) and two shells around the Zr (Al at 2.61-2.63 Å plus Al at 2.95-2.99 Å). To simulate also the secondary peaks in the FTs, calculations were performed with a more extended neighbourhood. Two types of clusters were used, one with the paths and degeneracies of a local face centered cubic (fcc) structure and one with the body centered cubic (bcc) values. Earlier simulations using the fcc cluster fit well with the EXAFS data for the alloys made with 0.5% V or Ti, and simulations using the bcc cluster fit the EXAFS data for alloys containing 2% Ti [12]. For the alloys doped with Zr, the two types of clusters give the same goodness of the fit while, for Hf, the fcc cluster gives better agreement. This is consistent with the two Zr-Al distances that are necessary to reconstruct the main peak in the FTs, while only one Hf-Al distance is needed. The fits for the fcc clusters are shown in figures 3 and 4 for the $k\chi(k)$ spectra and in fig. 5 and 6 for the FTs. In the Zr case, the FTs could be simulated up to 4.5 Å (uncorrected for phase shift), in the Hf case up to 5.5 Å. The structural parameters for the significant single paths in the fcc clusters model are listed in Table 1, along with the reliability factor, *RF*, which is a measure of the goodness of the fit. For Zr, they are also given, in Table 2, for the bcc cluster model.

The first interatomic distances are approximately 2.61 Å around a Zr atom; around Al they are 2.76 Å in the pure $Al_{88}Y_7Fe_5$ glass [12] and 2.8634 Å in α-Al. This nearest Zr-Al distance (2.61 Å) is noticeably shorter than the sum (3.03 Å) of the atomic radii of Zr and Al atoms (R_{Zr}= 1.60 Å; R_{Al}= 1.43 Å). The shortening is more drastic than in the cases of Ti and V; the relative shortening is 14% here while it was only 7% for Ti and 4 % for V. The nearest

Zr-Al distance compares better to the sum (2.66 Å) of the *covalent* radii of Zr and Al atoms (1.48 Å; 1.18 Å). Therefore, some covalent effect is evidenced in the Zr doped alloys.

The first Hf-Al distance (2.80 Å) is shorter than the sum (3.01 Å) of the atomic radii of Hf and Al atoms (R_{Hf}= 1.58 Å; R_{Al}= 1.43 Å). The relative shortening (7.6 %) is less significant than in the case of the Zr dopant. It has the same value as for the Ti-Al one in the alloy containing 0.5% Ti. The covalent bonding character for Zr and the possible bcc clustering around Zr atoms set Zr apart from the other Hf, Ti or V microadditions. This could reflect different electronic charge transfer from the Al-Al bond to the Al-TM bond associated with alloying, and to differences in the hybridization between the Al *p* and TM *d* electrons [22].

Many glasses are believed to contain strong icosahedral short-range order (ISRO), which is incompatible with crystalline periodicity. If microadditions enhance the ISRO, crystal nucleation will become more difficult and glass formation will be enhanced. This speculation is supported by a tendency for some Zr-based glasses (in the example: $Zr_{65}Al_{7.5}Ni_{10}Cu_{12.5}M_5$, where M is the microalloying element) to crystallize to the icosahedral phase when small amounts of noble elements such as Ag, Au, Pd and Pt [23] and the transition metals Nb, Ta, V [24] are added. Ag, Au, Pd, and Pt have strong negative heats of mixing with Zr, but interact only weakly with the Ni and Cu in the base alloy, suggesting that strongly bound icosahedral clusters may form around the transition metals, giving rise to strong ISRO in the liquid/glass.

To check this hypothesis, the EXAFS data was also fit with a local icosahedral cluster (a simple β-tungsten structure [25], cluster diameter about 1.1 nm). For the Hf, Ti, and V microadditions, the quality of the fits using this icosahedral cluster is equivalent to that of the fcc cluster; for Zr, the icosahedral fit is not as good (RF between 0.5 10^{-4} and 1.1 10^{-4}). Since very similar first neighbour distances were obtained for the fcc cluster and the icosahedral

cluster, the conclusions obtained above are applicable for either structure.

The fact that several cluster models can fit the data is rather puzzling. Of course, the first shell with a small disorder parameter, σ, could dominate the spectra so that the different clusters would be nearly identical. This is the case for Hf. However, in the Zr case, the second shell has also similar disorder value as the first one. For Hf, the fourth shell has the same disorder value as the first one. Therefore, the local order is not restricted to the first shell, as generally in metallic glasses, but extends farther. The distances obtained when using bcc or fcc clusters for Zr are the same within $\Delta R = 0.05$Å, which give us confidence in the distances. The major discrepancy between the models lays in the coordination numbers and in the disorder parameters, which are by no means independent parameters. The fit depends also on multiple scattering which is important here. In fact, the disorder parameter values of the multiple paths are of the same order as those of the simple paths. Without multiple scattering, the fit is less good. For example, using only the three simple paths in the Zr fcc cluster, the RF factor increases from $0.3\ 10^{-4}$ to $0.8\ 10^{-4}$ and $3\ 10^{-4}$ for respectively 0.5% and 1%. For Hf, the multiple scattering is useful to reproduce the FT between 3.7 and 5 Å. The fact that multiple scattering is not negligible in the cluster around minor additions means that the cluster is well structured. Several types of clusters, fcc and bcc ones around Zr, fcc and icosahedral ones around Hf, coexist probably in the alloy, as in the liquid melt.

Although the cluster size remains small, the model suggests that about 54 Al atoms are encaged in such a fcc cluster around a hafnium atom, 42 around a zirconium one. Taking into account the composition of the $Al_{87}Y_7Fe_5(Zr,Hf)_1$ alloy, this means that about 50 to 60 % of the Al are encaged in the fcc clusters and bound to Zr or Hf. Consequently, there are few “free” Al atoms that with annealing can form α-Al, the primary crystallizing phase. The clustering, therefore, removes regions in the melt in which α-Al can easily occur. This could also explain the shift to higher temperature for the formation of α-Al in the DSC experiments

[8, 10]. Further, in the case of Hf, the fits suggest that the local structure of the glass and liquid may contain some icosahedral short-range order, which is incompatible with crystalline periodicity, making crystal nucleation difficult and enhancing glass formation.

5. Discussion

The glass forming ability (GFA) of an alloy, upon cooling from its molten state, is strongly influenced by the effect on crystal nucleation of minor additions in the alloy melt [4-6,10,11]. To favour glass formation, the nucleation and growth of crystal phases should be suppressed during solidification. The presence of ordered nanoregions in an undercooled liquid state may give either a positive or negative effect on the GFA, depending on the similarities in structure and chemistry of the local order and of the nucleating crystal phases. If the local order in an undercooled liquid is similar to that of competing crystal phases, it will promote crystal nucleation and hence degrade the GFA. If it is dissimilar, however, it will raise the nucleation barrier and enhance the GFA. The latter is the case for the rapidly quenched Al-Y-Fe alloys that were doped with Ti or V [10-12], where the microadditions gave rise to a local structure of the liquid that was different from that of the primary crystallizing phase, α-Al, significantly enhancing glass formation. The emergence of new phases upon devitrification of alloys prepared with different microadditions that were studied here (figure 2) further supports the change in local structure that we observed in the EXAFS studies. Microalloying-induced ordering has been confirmed recently from high-energy synchrotron x-ray studies. Results from that study of microalloying with 3d transition metals in $Al_{88}Y_7Fe_5$ suggest that the ordering also decreases the atomic mobility in the glass, making nucleation more difficult [14].

These and our earlier EXAFS studies [12] show that although Ti, Zr and Hf are chemically similar group IV elements, microalloying with them yields glasses with different structures. The differences between Zr and Hf are particularly surprising because their atomic and ionic radii as well as their effective electronic structures are nearly identical, yet some alloys and compounds with Hf and Zf exhibit disparate properties. For example, Zheng, et al. have demonstrated that differences in the electronic structure of the respective oxides (TM-O_2) may be attributed to the greater electron affinity in the Hf compound over that in the Zr one [26]. Further, the heat of mixing of the Al-TM intermetallic phases is more negative in the Zr microalloys over those in the Ti and Hf containing glasses [22]. Similar effects could explain the increased shortening of Zr-Al bonds observed here.

6. Conclusion

The effects of the addition of a small amount of Zr and Hf on the atomic structure of Al-Y-Fe metallic glasses were examined using extended x-ray absorption fine structure (EXAFS) measurements of the Zr K and Hf LIII absorption edges. The local structure was determined around the Zr and Hf atoms. The same Al environment was found for the different concentrations of these microadditions, which could be modelled as a small cluster extending up to 4.5 Å around Zr atoms and up to 6 Å around Hf. Although the ordering effect is smaller in the Zr neighbourhood, a drastic shortening of the nearest Zr-Al distance is shown providing evidence for some covalent character, in line with the increase glass-forming ability found with Zr microaddition. This balance of ordering and shortening of the microaddition-Al bonds leads to varying degrees of increased glass forming ability and stability of the amorphous phase.

Acknowledgements

It is a pleasure to thank all the staff of the BM30B beam line for the experiments in ESRF. We also thank A. Michalowicz for the EXAFS programs. K. F. Kelton gratefully acknowledges support from the United States Air Force Office of Scientific Research, contract AFOSR FA9550-05-1-0110 and the National Science Foundation under DMR 06-06065.

References

[1] Z. P. Lu and C. T. Liu, J. Mat. Sci., **39**, 3965 (2004).

[2] C. T. Liu, C. L. White and J. A. Horton, Acta. Mater., **33**, 213 (1985).

[3] W. H. Wang, Z. Bian, P. Wen, Y. Zhang, M. X. Pan and D. Q. Zhao, Intermetallics, **10**, 1249 (2002).

[4] D. Xu, G. Duan and W. L. Johnson, Physical Review Letters, **92**, 245504 (2004).

[5] B. Zhang, R. J. Wang, D. Q. Zhao, M. X. Pan and W. H. Wang, Physical Review B **73**, 092201 (2006).

[6] Y. C. Kim, H. J. Chang, D. H. Kim, W. T. Kim and P. R. Cha, J. Phys. Condens. Matter **19**, 196104 (2007).

[7] Y. He, Y, S. J. Poon and G. J. Shiflet, Science, **241**, 1640 (1988).

[8] A.-P. Tsai, A. Inoue and T. Masumoto, Metall. Trans. A, **19A**, 1369 (1988).

[9] A. Inoue, N. Matsumoto and T. Masumoto, Mater. Trans. JIM, **31**, 493 (1990).

[10] L. Q. Xing, A. Mukhopadhyay, W. E. Buhro and K. F. Kelton, Phil. Mag. Let. **84**, 293 (2004).

[11] A. Mukhopadhyay, K. E. Spence, L. Q. Xing, W. E. Buhro, K. F. Kelton, Phil. Mag. **87**, 281 (2007).

[12] A. Sadoc, O. Heckmann, V. Nassif, O. Proux, J.-L. Hazemann, L. Q. Xing, K. F. Kelton, J. Non Cryst. Solids, **353**, 2758 (2007).

[13] O. Proux, V. Nassif, A. Prat, O. Ulrich, E. Lahera, X. Biquard, J.-J. Menthonnex and J.-L. Hazemann, Journal of Synchrotron Radiation **13**, 59 (2006).

[14] K. S. Bondi, A. K. Gangopadhyay, Z. Marine, T. H. Kim, A. Mukhopadhyay, A. I. Goldman, W. E. Buhro, K. F. Kelton, J. Non-Cryst. Solids, **353**, 4723 (2007).

[15] A. Michalowicz, EXAFS pour le MAC, in *Logiciels pour la Chimie*, edited by

Société Française de Chimie, (Paris, 1991) p. 102. A. Michalowicz, J. Phys. IV, France, **7**, C2-235 (1997). http://www.univ-paris12.fr/lps2m/

[16] J. J. Rehr and R. C. Albers, Reviews of Modern Physics **72**, 621 (2000); J. J. Rehr and A. Ankudinov, J. Synchrotron Rad., **10**, 43 (2003).

[17] M. Newville, P. Livins, Y. Yacoby, J. J. Rehr and E. A. Stern, Phys. Rev. B **47**, 14126 (1993); S. I. Zabinsky, J. J. Rehr, A. Ankudinov, R. C. Albers and M. J. Eller, Phys. Rev. B **52**, 2995 (1995); M. Newville, R. Ravel, D. Haskel, J. J. Rehr, E. A. Stern and Y. Yacoby, Physica B **208-209**, 1547 (1995).

[18] R. W. G. Wyckoff, *Crystal Structures* (John Wiley & Sons, New York, London, 1963) vol. 1.

[19] K. Saksl, P. Jovari and H. Franz, J. Appl. Phys., **97**, 113507 (2005).

[20] D. B. Miracle, W. S. Sanders and O. N. Senkov, Phil. Mag., **83**, 2409 (2003).

[21] K. Saksl, J. Bednarcik, R. Nicula, E. Burkel, S. Roth and H. Franz, J. Phys.: Condens. Matt., **19,** 176215 (2007).

[22] J. Z. Liu, G. Ghosh, A. van de Walle, M. Asta, Phys. Rev. B., **75**, 104117 (2007).

[23] A. Inoue, T. Zhang, J. Saida, M. Matsushita, M. Chen, and T. Sakurai, Mat. Trans. JIM, **40,** 1181 (1999)**.**

[24] J. Saida, J. Phys.: Condens. Matt., **13,** L73 (2001).

[25] V. Nevitt, in Intermetallic Compounds, J. H. Westbrook, ed., (John Wiley & Sons, New York, 1967) Ch. 13.

[26] W. Zheng, K. H. Bowen, Jr., J. Li, I. Dabkowska, and M. Gutowski, Journal of Physical Chemistry A **109**, 11521 (2005).

Figure captions

Figure 1. a) Nonisothermal DSC scans of the rapidly-quenched alloys containing the Zr and Hf microadditions. b) Expansion of the regions around the glass transition temperature, T_g, (when present) (downward-pointing arrows) and T_x, the primary crystallization temperature (upward-pointing arrows); relative temperature ranges are shifted for better comparison, showing the 90 ºC near T_x.

Figure 2. Isothermal DSC scans for the rapidly-quenched alloys containing the Zr and Hf microadditions. The numbers indicate the isothermal annealing temperatures (C).

Figure 3. The $k\chi(k)$ EXAFS spectra for the Zr K absorption edge of a zirconium foil and of $Al_{88-x}Y_7Fe_5Zr_x$ for x = 0.5, 1 and 2%. Dots represent the experimental data and lines represent the best fit.

Figure 4. The $k\chi(k)$ EXAFS spectra for the Hf LIII absorption edge of a hafnium foil and of $Al_{88-x}Y_7Fe_5Hf_x$ for x = 1, 2 and 3%. Dots represent the experimental data and lines represent the best fit.

Figure 5. Moduli of the Fourier transforms of the EXAFS spectra as a function of distance (Å) for the Zr K absorption edge of a zirconium foil and of $Al_{88-x}Y_7Fe_5Zr_x$ for x = 0.5, 1 and 2%. Dots represent the experimental data and lines represent the best fit.

Figure 6. Moduli of the Fourier transforms of the EXAFS spectra as a function of distance (Å) for the Hf LIII absorption edge of a hafnium foil and of $Al_{88-x}Y_7Fe_5Hf_x$ for x = 1, 2 and 3%.

Dots represent the experimental data and lines represent the best fit.

Figure 1, Sadoc et al.

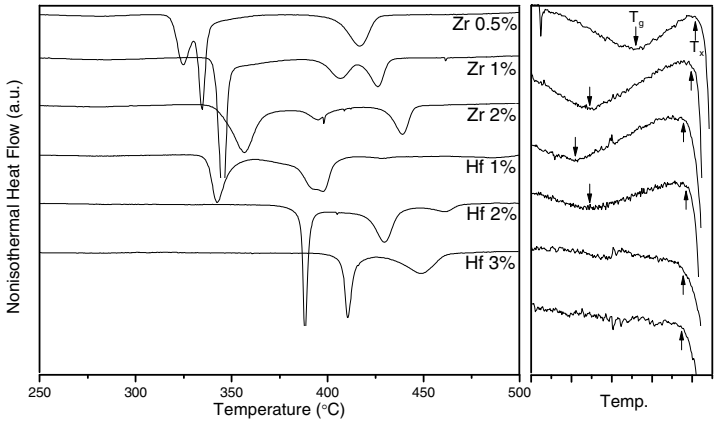

Figure 2, Sadoc et al.

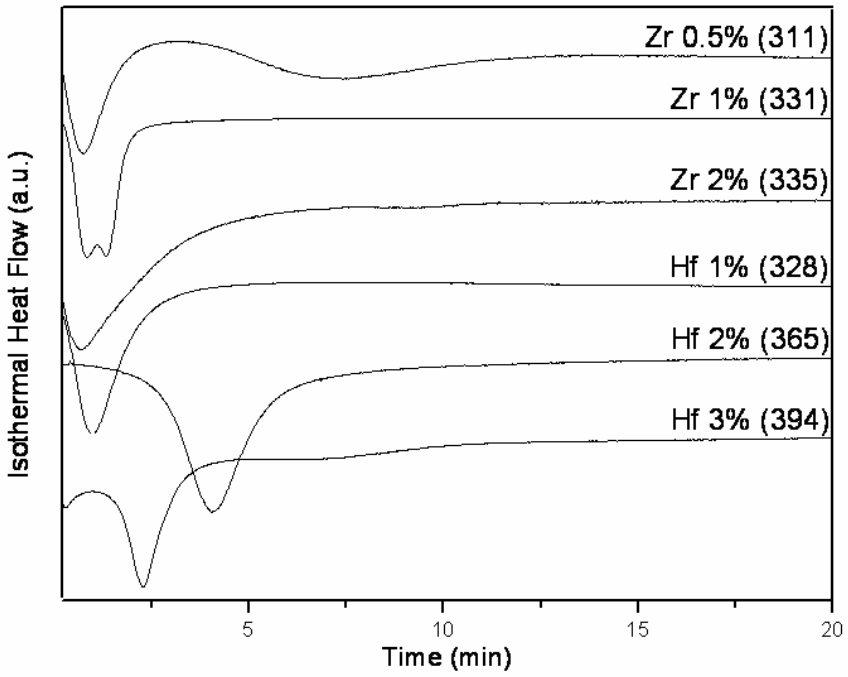

Figure 3, Sadoc et al.

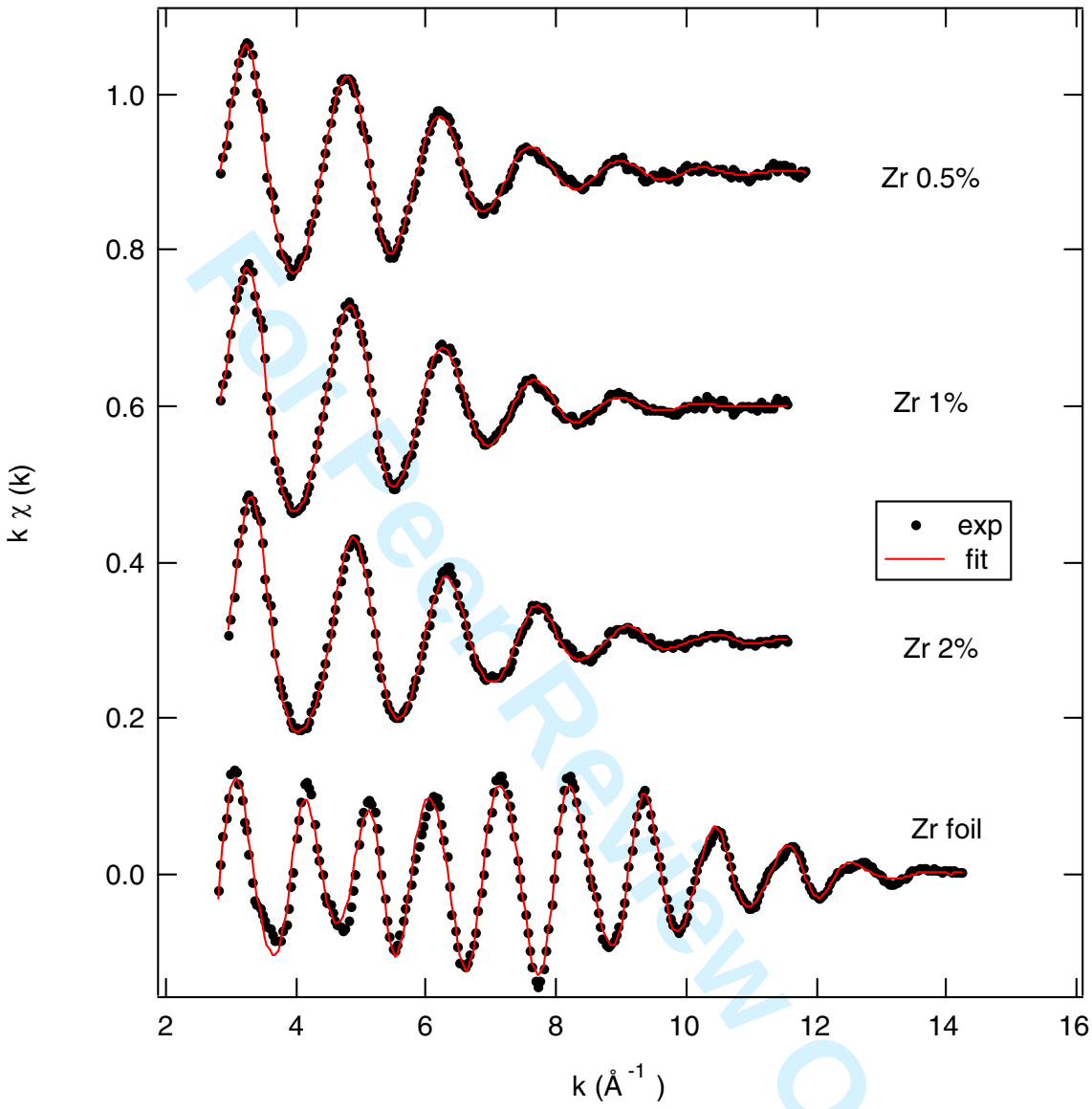

Figure 4, Sadoc et al.

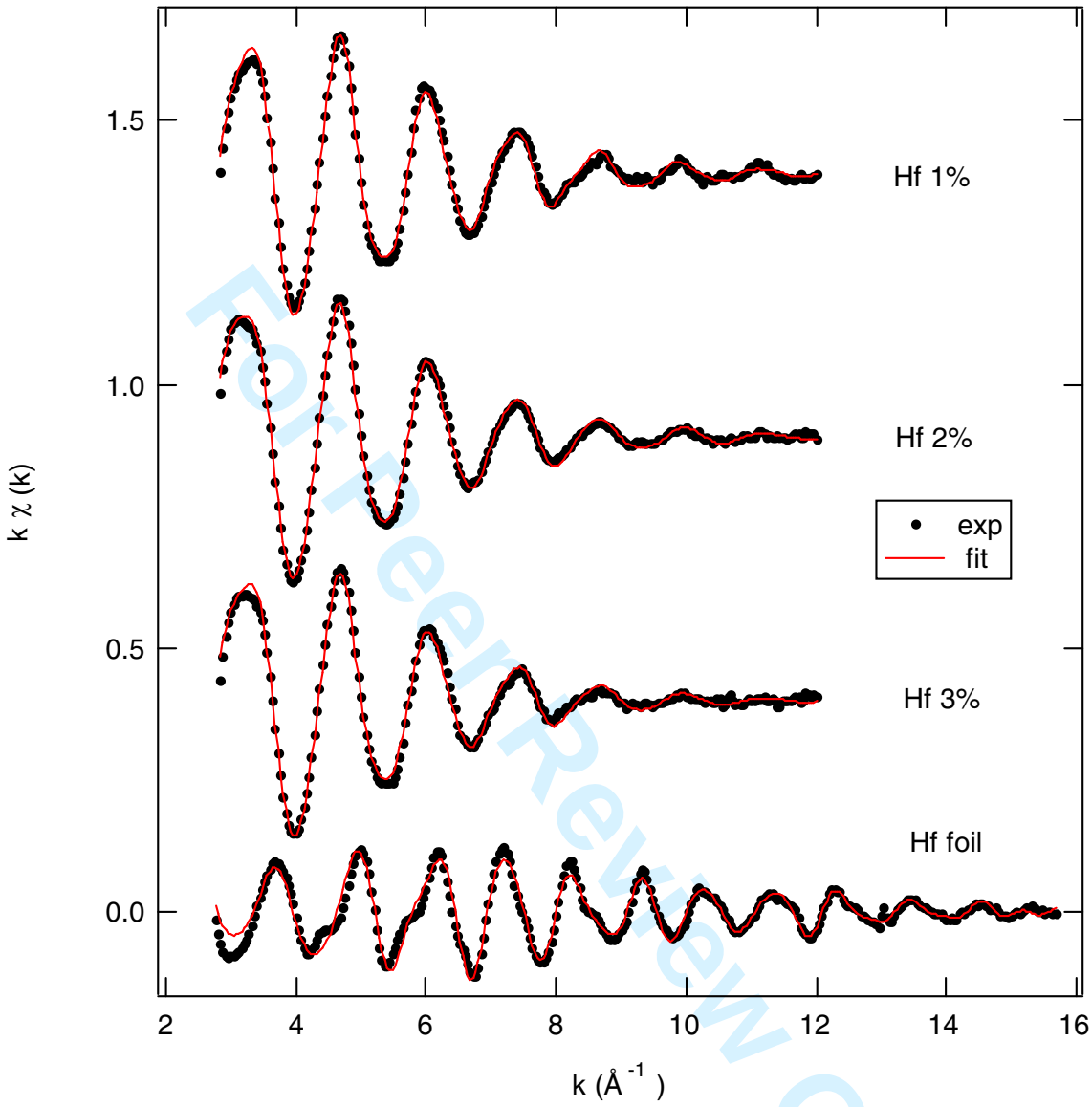

Figure 5, Sadoc et al.

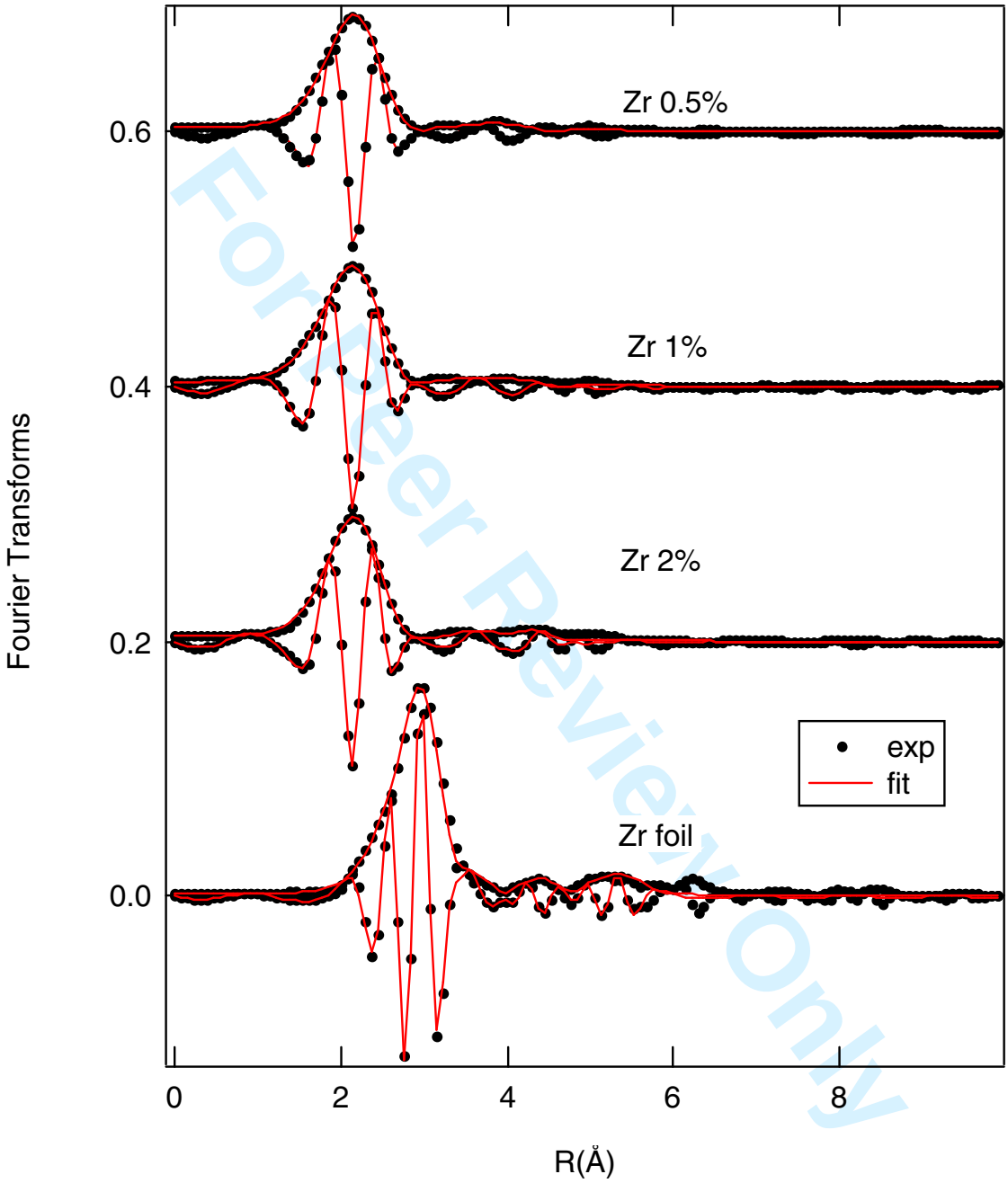

Figure 6, Sadoc et al.

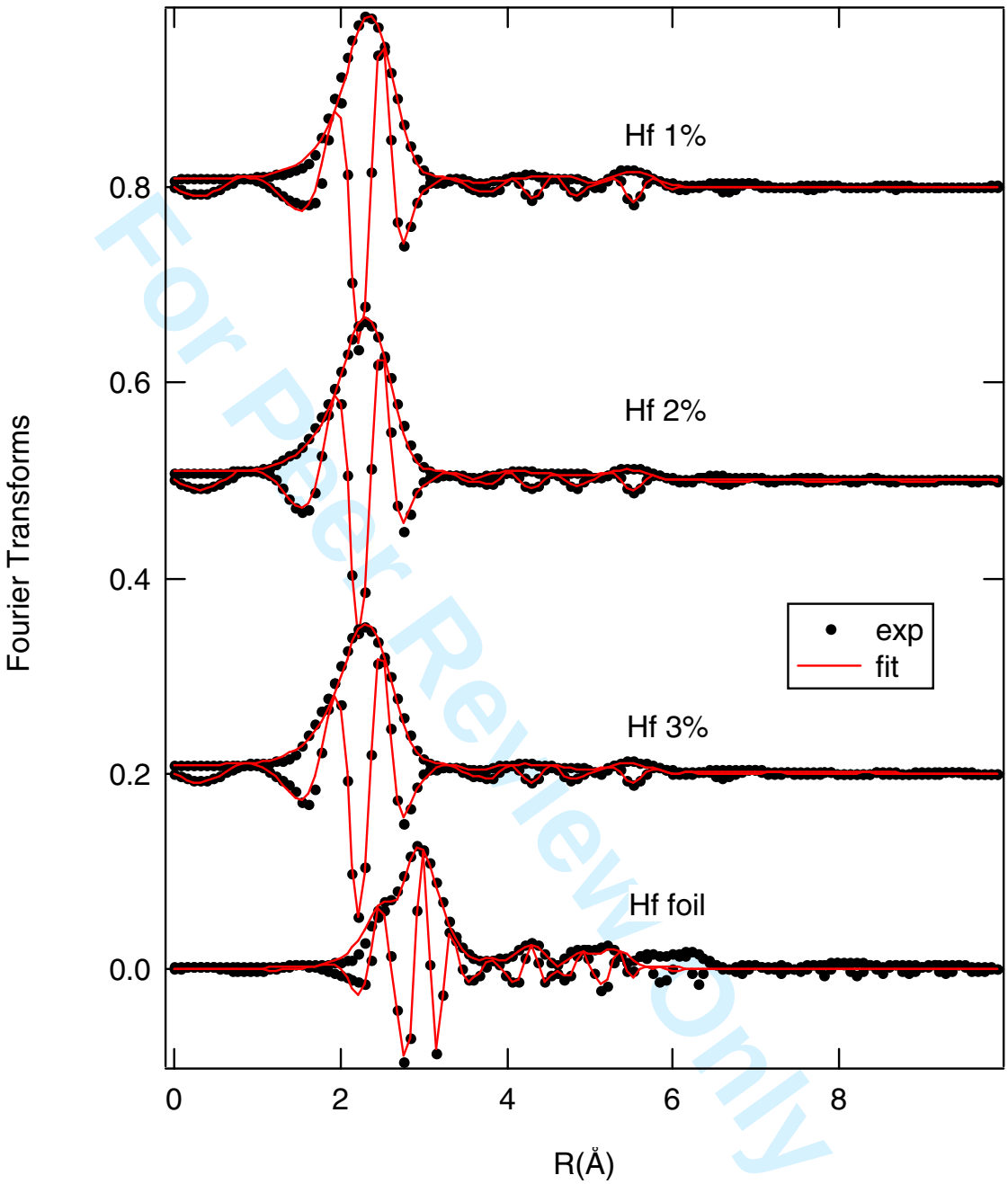

Table 1: Fcc cluster: first environments around Hf and Zr atoms in $Al_{88-x}Y_7Fe_5(Zr, Hf)_x$ alloys compared to those around Ti and V [12]. RF is the goodness of the fit. N is the number of Al neighbours, R(Å) their distance from the central atom and σ^2(Å^2) the mean relative displacement. The error bars are of the order of $\Delta R = 0.05$Å and $\Delta\sigma^2 = 0.005$ Å^2.

	Hf 1 %		Hf 2 %		Hf 3 %		Zr 0.5 %		Zr 1 %		Zr 2 %		Ti 0.5 %		V 0.5 %	
N	R(Å)	σ^2(Å^2)	R(Å)	σ^2(Å^2)	R(Å)	σ^2(Å^2)	R(Å)	σ^2(Å^2)	R(Å)	σ^2(Å^2)	R(Å)	σ^2(Å^2)	R(Å)	σ^2(Å^2)	R(Å)	σ^2(Å^2)
12	2.80	0.010	2.78	0.011	2.79	0.012	2.63	0.017	2.60	0.019	2.61	0.015	2.69	0.005	2.65	0.007
6	4.21	0.033	4.23	0.021	4.18	0.040	2.96	0.017	2.98	0.015	2.92	0.017	4.19	0.015	4.08	0.050
24	4.92	0.027	5.00	0.044	4.86	0.028	4.47	0.064	4.38	0.075	4.58	0.071	4.76	0.014	4.68	0.012
12	6.03	0.010	5.98	0.016	6.00	0.017							5.57	0.006	5.56	0.008
RF	$0.11\ 10^{-3}$		$0.6\ 10^{-4}$		$0.1\ 10^{-3}$		$0.3\ 10^{-4}$		$0.3\ 10^{-4}$		$0.3\ 10^{-4}$		$1.5\ 10^{-3}$		$0.5\ 10^{-3}$	

Table 2: bcc cluster: first environments around Zr atoms in $Al_{88-x}Y_7Fe_5Zr_x$ alloys. RF is the goodness of the fit. N is the number of Al neighbours, R(Å) their distance from the central atom and σ^2(Å^2) the mean relative displacement. The error bars are of the order of $\Delta R = 0.05$Å and $\Delta\sigma^2 = 0.005$ Å^2.

	Zr 0.5 %		Zr 1 %		Zr 2 %	
N	R(Å)	σ^2(Å^2)	R(Å)	σ^2(Å^2)	R(Å)	σ^2(Å^2)
8	2.61	0.013	2.58	0.015	2.59	0.011
6	3.04	0.036	3.04	0.019	3.00	0.028
12	4.42	0.052	4.40	0.043	4.48	0.036
RF	$0.3\ 10^{-4}$		$0.3\ 10^{-4}$		$0.3\ 10^{-4}$	